Separation Science and Technology
Publication details, including instructions for authors and subscription information:
http://www.informaworld.com/smpp/title~content=t713708471

Separation of Cesium and Strontium from Acidic Radioactive Waste Simulants Using a Microporous Tungstate/Polyacrylonitrile (PAN) Composite Adsorbent

Christopher S. Griffith[a]; Vittorio Luca[a]; Ferdinand Šebesta[b]; Patrick Yee[a]
[a] Australian Nuclear Science and Technology Organisation, Menai, NSW, Australia [b] Department of Nuclear Chemistry, Czech Technical University in Prague, Prague Brehová, Czech Republic

To cite this Article Griffith, Christopher S. , Luca, Vittorio , Šebesta, Ferdinand and Yee, Patrick(2005) 'Separation of Cesium and Strontium from Acidic Radioactive Waste Simulants Using a Microporous Tungstate/Polyacrylonitrile (PAN) Composite Adsorbent', Separation Science and Technology, 40: 9, 1781 — 1796
To link to this Article: DOI: 10.1081/SS-200064561
URL: http://dx.doi.org/10.1081/SS-200064561

Separation Science and Technology, 40: 1781–1796, 2005

ISSN 0149-6395 print/1520-5754 online
DOI: 10.1081/SS-200064561

Separation of Cesium and Strontium from Acidic Radioactive Waste Simulants Using a Microporous Tungstate/Polyacrylonitrile (PAN) Composite Adsorbent

Christopher S. Griffith, Vittorio Luca, and Patrick Yee
Australian Nuclear Science and Technology Organisation, Menai, NSW, Australia

Ferdinand Šebesta
Department of Nuclear Chemistry, Czech Technical University in Prague, Prague Brehová, Czech Republic

Abstract: The inorganic phase, $Na_{0.2}Mo_{0.03}W_{0.97}O_3 \cdot ZH_2O$ (MoHTB), which has been previously shown to be selective for Cs^+ and Sr^{2+} from acidic radwaste simulants ($0.075\,mmol \cdot L^{-1}$, 1.0 M HNO_3), has been granulated with polyacrylonitrile (PAN) to afford a composite adsorbent suitable for deployment in small scale, fixed-bed columns. The uptake of Cs^+ and Sr^{2+} by the MoHTB-PAN composites from such an acidic radwaste simulant is optimal for granular material of mesh size <0.3 mm but satisfactory uptake rates are also observed with material of mesh size 0.3–0.63 mm. The fixed-bed column adsorption of Cs^+ and Sr^{2+} from acidic radwaste simulant affords breakthrough curves which are of a typical 'S' shape profile but desorption of adsorbed Sr^{2+} by Cs^+ in the radwaste simulant occurs after the composite column achieves equilibrium with respect to Sr^{2+}. A simplified model of the adsorption of Cs^+ and Sr^{2+} by the MoHTB-PAN composite fixed-bed column has been applied to these initial results and has been shown to have utility in describing the performance of the fixed-bed column setup at the equimolar concentrations of Cs^+ and Sr^{2+} employed.

Keywords: Ion-exchange, radwaste, cesium, strontium, composite adsorbent, fixed-bed adsorption

Received 29 November 2004, Accepted 4 August 2005
Address correspondence to Christopher S. Griffith, Australian Nuclear Science and Technology Organisation, PMB 1, Menai, NSW 2234, Australia. Tel.: 61-2-9717 3923; Fax: 61-2-9543 7179; E-mail: cgz@ansto.gov.au

INTRODUCTION

In recent years there has been a considerable effort directed toward the development of inorganic ion-exchange materials for the removal of aqueous metal cations in a range of applications (1). One of the major drivers for these investigations has been the fact that such ion-exchangers generally display superior selectivity for given aqueous metal cations over that of the more traditional organic-based ion-exchange resins, even in the presence of high concentrations of competing cations viz. Na^+, K^+, H_3O^+. Furthermore, where the remediation of radioactive waste ('radwaste') streams are the targeted application, inorganic ion-exchangers generally display superior radiation stability.

Given these potential advantages, it not surprising that numerous researchers have focused on the development of inorganic ion-exchangers for the selective removal (pretreatment) of both ^{137}Cs and ^{90}Sr from alkaline and acidic radwaste, as these two radionuclides account for the majority of activity in older (>4 y) waste streams from reprocessing and ^{99}Mo production facilities. Such pretreatment can potentially concentrate the majority of the activity onto a relatively small volume of sorbent, aiding in the management and costs associated with such wastes (2). The considerable effort required to develop materials with this prerequisite selectivity for ^{137}Cs and ^{90}Sr is exemplified by the crystalline silico-titanate (CST) ion-exchanger (commercial name—UOP IONSIV IE-910 [powder] and −911 [granular form], UOP, Inc. Des Plains, IL.) which has proven utility in the pretreatment of highly alkaline solutions containing molar quantities of competing cations eg. Na^+ (3–6). However, to date, there have been no reports of a granular inorganic ion-exchanger which displays good selectivity for both ^{137}Cs and ^{90}Sr in highly acidic solutions. Commonly, materials which display selectivity for Cs^+ in acidic solutions do not display selectivity for Sr^{2+}, and vice versa.

Recent investigations by our group on the possible pretreatment of acidic radwaste resulting from the Brookhaven alumina-nitric acid separation of ^{99}Mo using the microporous tungstate phase, $Na_{0.2}Mo_{0.03}W_{0.97}O_3 \cdot ZH_2O$ (MoHTB), have shown that this inorganic phase displays promising selectivity for both Cs^+ and Sr^{2+} from acidic (1.0 M HNO_3) radwaste simulants (7, 8). Although this adsorbent may hold some utility for the pretreatment of this waste, or that arising from future advanced nuclear fuel cycles, the microcrystalline nature of the material precludes its direct deployment in fixed-bed column separations. This issue is common to many inorganic ion-exchangers and has been in part overcome for several of these materials through granulation with polyacrylonitrile (PAN) (9).

Herein we wish to report on the granulation of the MoHTB phase with polyacrylonitrile and the basic adsorption performance of the composite adsorbent for removal of Cs^+ and Sr^{2+} from acidic radwaste simulants. Initial investigations of the fixed-bed column performance of this material with similar radwaste simulant clearly indicates the potential of the composite adsorbent

in addressing the removal of ^{137}Cs and ^{90}Sr from selected acidic radwaste streams.

EXPERIMENTAL

Standard laboratory grade (>99% purity) $Cs(NO_3)$ and $Sr(NO_3)_2$ from Sigma Aldrich and concentrated HNO_3 from Ajax Chemicals were employed for the preparation of stock solutions. The inorganic adsorbent, $Na_{0.2}Mo_{0.03}W_{0.97}O_3 \cdot ZH_2O$ (MoHTB), was synthesized as described previously (10–12). The composite adsorbent, ammonium molybdophosphate/polyacrylonitrile (AMP-PAN-85—85.7% w/w, 0.5–1.0 mm bead size), was supplied by the Czech Technical University in Prague.

Micrographs of the MoHTB-PAN composite adsorbents were obtained using a JEOL 6400 m scanning electron microscope operating at 15 kV, on carbon-coated, sectioned samples mounted on a graphite block. Elemental analysis of cation-containing acidic solutions was performed on a Perkin Elmer *Elan 6100* Inductively Coupled Plasma Mass Spectrometer (ICPMS). Surface area measurements were collected on a Micrometrics ASAP 2010 porosimeter.

Synthesis of $Na_{0.3}Mo_{0.03}W_{0.97}O_3 \cdot ZH_2O$/polyacrylonitrile (MoHTB-PAN)

The MoHTB-PAN-*x* composite adsorbents ($x = 80\%$ w/w) were synthesized by coagulation of a mixture of PAN and MoHTB adsorbent in dimethyl sulphoxide, in an aqueous bath in the manner outlined previously for the synthesis of other PAN-based composite adsorbents (13, 14). The resultant granular materials were wet-sieved into the size fractions >0.8, 0.63–0.80, 0.30–0.63 and <0.3 mm (MoHTB-PAN-80-A, -B, -C, and -D, respectively). The percentage weight loading of the inorganic adsorbent was determined by thermogravimetric analysis and monitoring the weight loss on thermal decomposition of the PAN matrix. Beads were stored in the absence of light and at ambient temperature.

Static Batch Contact Ion-Exchange

The simple ion-exchange behavior of the MoHTB-PAN-80 composite adsorbents was investigated using the batch contact method. Typically, composite adsorbent beads (230 mg) and radwaste simulant solution (20 mL, ca. 0.075 mM Cs^+/Sr^{2+} in 1 M HNO_3) were contacted at $25 \pm 1^\circ C$, with agitation (platform shaker), for between 5 and 480 min. (kinetic experiments) or 1440 min. (equilibrium experiments). A V (mL): m (g) ratio of 100 mL $\cdot$ g^{-1} was engineered into all experiments to allow meaningful comparison of Cs^+ and Sr^{2+} extraction levels. After the specified contact time, the supernatant was removed, syringe filtered (0.45 μm), and the metal cation concentrations

analyzed by ICPMS. Determination of the metal cation concentrations before and after contact with the composite adsorbent allowed calculation of the extraction level via the formula

$$\%_{extraction} = \frac{(C_i - C_f)}{C_i} \cdot 100 \quad (1)$$

where C_i and C_f are the initial and final cation concentrations, respectively. The concentrations of Cs^+ and Sr^{2+} employed in these investigations (0.075 mM) are indicative of the concentrations of ^{137}Cs and ^{90}Sr present in the older acidic waste from ^{99}Mo production at the Australian Nuclear Science and Technology Organisation (ANSTO) site.

Fixed-Bed Column Performance Evaluation

Composite adsorbent columns of ca. 0.8 ml bed volume (BV; 0.5 [internal diameter] × 4.0 cm) were utilized to determine the dynamic capacities and kinetics of Cs^+ and Sr^{2+} removal from radwaste simulant solutions (ca. 0.075 mM Cs^+/Sr^{2+} in 1.0 M HNO_3). Columns were constructed of a stainless steel (L316C—low carbon) body, fitted with stainless steel (L316C—low carbon) Swagelock hose reducer adapters at the inlet and outlet of the column. Stainless steel (L316) mesh (50 μm) inserts were fixed inside the inlet and outlet adapters to support the bed of composite adsorbent. The mass of composite adsorbent employed in each test was measured externally. Columns were loaded with dry adsorbent using careful and intermittent agitation to ensure uniform packing throughout the column. Once connected to the experimental setup, which had already been flushed with Millipore water to exclude air, Millipore water was then pumped through the column (200 mL, 20 mL · min^{-1}) by a precalibrated, Masterflex peristaltic pump to exclude air from the adsorbent bed. The composite adsorbent columns were then conditioned with 1.0 M HNO_3 (50 mL, 1.0 mL · min^{-1}) before the column feed line was switched to the simulant solution and pumped through the column at a flow rate of 30 BV · h^{-1}. To ensure consistent flow rates during each experiment, calibration of the peristaltic pump was conducted before and after each test. Column eluant was collected by a fraction collector (Eldex universal fraction collector, Eldex Corporation, USA) and the concentration of Cs^+ and Sr^{2+} in given fractions determined by ICPMS.

RESULTS AND DISCUSSION

MoHTB-PAN–80 Composite Adsorbents

The SEM micrographs of the cross-sections of the granular MoHTB-PAN-80-C ($0.3 < x < 0.63$ mm) composite adsorbent prepared by the coagulation of a mixture of MoHTB and PAN in an aqueous bath are shown in Fig. 1a. The

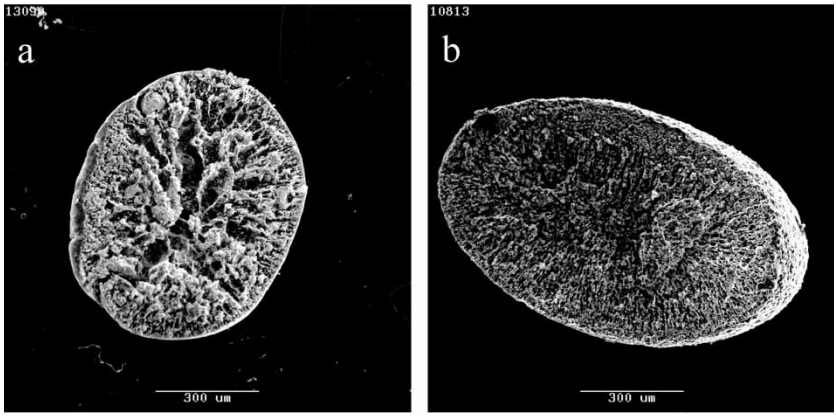

Figure 1. SEM (secondary electron) micrographs of the cross-section of (a) MoHTB-PAN-80-C (0.3–0.63 mm) composite adsorbent; and (b) AMP-PAN-85 (0.5–1.0 mm) composite adsorbent.

internal structure displayed by this bead size fraction is also indicative of those of the other bead size fractions produced by this method. The micrographs highlight that the macroporous internal structure observed for the MoHTB-PAN-80 composites is comparable to that of AMP-PAN-85 (Fig. 1b) with interconnecting pores radiating outwards from the center of the beads. The N_2 adsorption data presented in Table 1 further highlight the open structure of the MoHTB-PAN-80 and AMP/PAN-85 composites with between 31–36 $m^2 \cdot g^{-1}$ of surface area (excluding microporosity) measured for each of the size fractions. The pore size distribution of the MoHTB-PAN-80-D (<0.3 mm) composite as determined from the N_2 adsorption data is given in Fig. 2 along with the N_2 adsorption and desorption isotherm plot. This

Table 1. Various physical properties of MoHTB-PAN and AMP-PAN-85 composite adsorbents

		MoHTB/PAN composites (mm)			
	AMP/PAN 0.5–1.0 mm	80% >0.8	80% 0.63–0.8	80% 0.3–0.63	80% <0.3
Surface area total ($m^2 \cdot g^{-1}$)	132	37.5	39.8	41.1	41.8
Surface area (ex. micro.) ($m^2 \cdot g^{-1}$)	31.6	34.0	35.5	36.3	36.8
Density ($g \cdot mL^{-1}$)	0.614	0.269	0.272	0.279	0.334

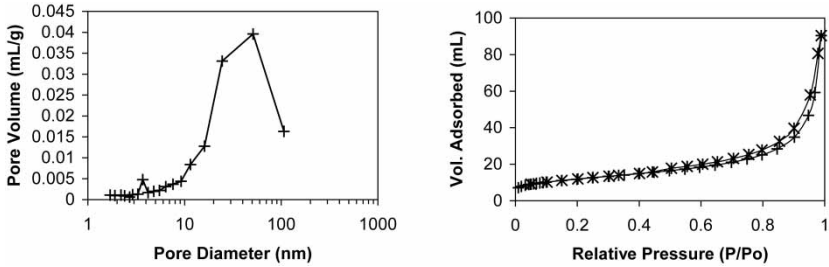

Figure 2. Pore size distribution of MoHTB-PAN-80-D (<0.3 mm) (left) as determined by N_2 adsorption/desorption isotherms (right).

data is indicative of the remaining size fractions of the MoHTB-PAN-80 composite. The distribution data show that the composite matrix contains a very small fraction of mesoporosity with a narrow pore diameter range of between 3.5–4.5 nm; however, a majority of the porosity of the composite is defined as macroporous consisting of a relatively broad distribution of pore sizes between 20–100 nm.

In order to determine the most appropriate form of the composite adsorbent for fixed-bed column separations and determine the effect that bead size has on the uptake of Cs^+ and Sr^{2+} from acidic solution as a function of time, the kinetic profiles for the adsorption of Cs^+ (Fig. 3) and Sr^{2+} (Fig. 4) were determined for each of the MoHTB-PAN-80 composites.

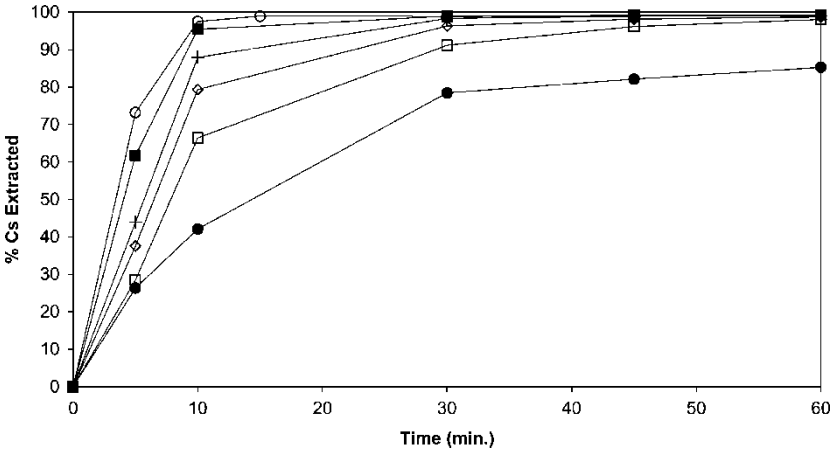

Figure 3. Time dependent Cs^+ sorption profiles for MoHTB-PAN-80 and AMP-PAN-85 composite adsorbents with radwaste simulant (ca. $0.075\,mmol \cdot L^{-1}$ Cs^+ and Sr^{2+} in 1.0 M HNO_3; $V/m = 100\,ml \cdot g^{-1}$). Legend: >0.8 mm (□); 0.63–0.8 mm (◇); 0.3–0.63 mm (+); <0.3 mm (■); AMP-PAN-85 (●) and powdered MoHTB (○).

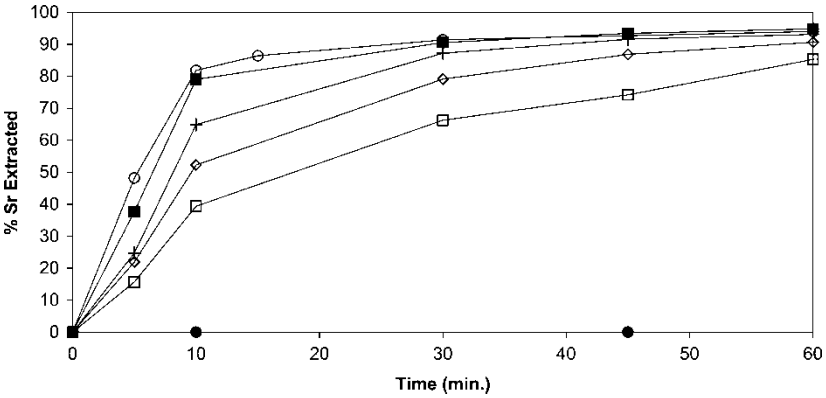

Figure 4. Time-dependent Sr^{2+} kinetic profiles for MoHTB-PAN-80 and AMP-PAN-85 composite adsorbents with radwaste simulant (ca. $0.075\,mmol \cdot L^{-1}$ Cs^+ and Sr^{2+} in 1 M HNO_3; $V/m = 100\,ml \cdot g^{-1}$). Legend: >0.8 mm (□); 0.63–0.8 mm (◇); 0.3–0.63 mm (+); <0.3 mm (■); AMP-PAN-85 (●) and powdered MoHTB (○).

The kinetic profile for Cs^+ uptake by AMP-PAN-85 was also determined in parallel for comparison against the MoHTB-PAN-80 composites. The MoHTB-PAN-80-D composite (<0.3 mm) displays the fastest uptake of Cs^+ and is comparable with the uptake displayed by the parent MoHTB sorbent (○). The next largest size fraction, MoHTB-PAN-80-C (0.3–0.63 mm), sorbs ca. 15% and 5% less Cs^+ at 5 and 10 min. contact, respectively. However, maximum uptake of Cs^+ is still observed at 30 min. contact. Both the MoHTB-PAN-80-B (0.63–0.8 mm) and MoHTB-PAN-80-A (>0.8 mm) display similar uptake profiles but only attain maximum uptake of Cs^+ after 60 min. contact. Importantly, the extensively investigated AMP-PAN-85 composite displays slower uptake of Cs^+ than all of the MoHTB-PAN-80 composites, only reaching maximum uptake after 100 min. contact. However, this may be attributed to the fact that the material had been air-dried after coagulation, and optimum uptake for this material is known to occur only with beads that remain wet after coagulation (15).

In a similar fashion to the uptake of Cs^+, the MoHTB-PAN-80-D composite displays the fastest uptake of Sr^{2+}, reaching maximum uptake at ca. 60 min. contact (Fig. 4). The rate of Sr^{2+} uptake, in comparison to that of Cs^+, is considerably slower for this material and this property has been reported previously (7, 8). The remaining MoHTB-PAN-80 composites all display comparable uptake profiles, attaining maximum uptake of Sr^{2+} between 60–240 min. contact. The lack of uptake by AMP-PAN-85 for Sr^{2+} is consistent with the well-known behavior of this phase.

The rate of uptake of Cs^+ and Sr^{2+} by the composite adsorbents can also be compared via numerical treatment using a pseudo-second order rate law first proposed by Ho et al. (16) (Eq. 2). The rate constant k_{ad} for Cs^+ and

Table 2. Pseudo second order rate constants for the adsorption of Cs^+ and Sr^{2+} by MoHTB, AMP-PAN-85 and MoHTB-PAN-80 composite adsorbents from radwaste simulant

	Cs^+		Sr^{2+}	
	k_{ad} ($g \cdot mg^{-1}$ min.)	h ($mg \cdot g^{-1}$ min.)	k_{ad} ($g \cdot mg^{-1}$ min.)	h ($mg \cdot g^{-1}$ min.)
MoHTB	5.29	0.716	6.25	0.0544
MoHTB-PAN-80-A	1.01	0.120	0.894	0.0068
MoHTB-PAN-80-B	1.33	0.156	1.53	0.0117
MoHTB-PAN-80-C	3.01	0.342	2.74	0.0202
MoHTB-PAN-80-D	3.64	0.411	5.47	0.0394
AMP-PAN-85	0.644	0.0202	nd	nd

nd: not determined.

Sr^{2+} adsorption by the MoHTB-PAN-80-D composite supports the graphical assessment of the two uptake profiles against the other composites as discussed previously (Table 2). The constant h is defined by Eq. (3) and represents the rate of adsorption by the various composite sorbents as $t(\text{min}) \rightarrow 0$. For the MoHTB-PAN-80-D composite, both k_{ad} and h approach that of the parent MoHTB, thus demonstrating that the PAN matrix impacts minimally upon the adsorption properties of the sorbent at this bead size but is still the limiting factor to the rate of uptake. To test the utility of the MoHTB-PAN material in a fixed-bed column setup, the MoHTB-PAN-80-D (<0.3 mm) and MoHTB-PAN-80-C (0.3–0.63 mm) materials were selected for further investigation.

$$\frac{t}{q_t} = \left(\frac{1}{k_{ad} q_e}\right) + \left(\frac{1}{q_e}\right) \cdot t \tag{2}$$

$$h \cong k_{ad} q_e^2 \quad \text{as } t \rightarrow 0 \text{ min} \tag{3}$$

Fixed-Bed Column Performance of MoHTB-PAN-80-C (0.3–0.63 mm) and -D (0.3 mm) Composite Adsorbents

The Cs^+ and Sr^{2+} breakthrough profiles for the MoHTB-PAN-80-C and -D composite columns conducted at $30\,BV \cdot h^{-1}$ with acidic radwaste simulant are presented in Fig. 5. If column breakthrough for Cs^+ and Sr^{2+} is defined at the 1% level, the profiles demonstrate breakthrough at ca. 180 and 600 BV, respectively, for the MoHTB-PAN-80-C, and 350 and 1000 BV, respectively, for the MoHTB-PAN-80-D composite. Exhaustion (>95%

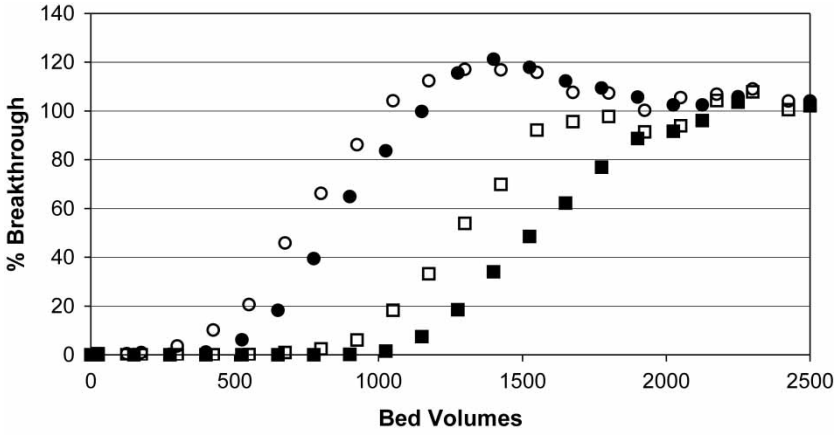

Figure 5. Breakthrough profiles of Cs^+ and Sr^{2+} for MoHTB-PAN-80-C and -D composite fixed-bed columns using acidic radwaste simulant (ca. 0.075 mmol · L^{-1} Cs^+ and Sr^{2+} in 1.0 M HNO_3); BV = ca. 0.8 ml; F = 30 BV · h^{-1}; Legend: MoHTB-PAN-80-D – Cs^+ and Sr^{2+} (■ and ●, respectively), MoHTB-PAN-80-C – Cs^+ and Sr^{2+} (□ and ○, respectively).

breakthrough) of both columns with respect to Cs^+ is observed within 1300 BV from the point of breakthrough, and with respect to Sr^{2+}, within 800 BV. The earlier breakthrough observed for Sr^{2+} is expected, as the capacity of the MoHTB sorbent for Sr^{2+} is known to be ca. 50% (on a mmol · g^{-1} basis) of that for Cs^+ from our previous investigations (7, 8). It is mindful at this stage to consider that on the basis of previous investigations of the AMP-PAN-85 composite one would predict breakthrough of Cs^+, by a similar size column with this simulant, at significantly higher bed volumes. Importantly though, no Sr^{2+} would be removed from the simulant unlike the MoHTB-PAN-80 composite column.

The four breakthrough profiles in Fig. 5 all appear as typical 'S' shaped curves between 0–95% breakthrough. However, in the case of the Cs^+ breakthrough profiles there is a slight flattening, or decrease in the slope, of the curves between 1–90% breakthrough in comparison to that of the corresponding Sr^{2+} breakthrough curves. Furthermore, at ca. 95% breakthrough there is a second flattening of the Cs^+ breakthrough curves which significantly increases the number of BV of simulant required before the fixed-beds reach equilibrium. We postulate that this flattening at high breakthrough represents a slowing in the kinetics associated with the adsorption of Cs^+ as the composite struggles to adsorb the maximum level of Cs^+. Also evident from Fig. 5 is that as passage of the feed simulant continues past the point where the fixed-beds attain equilibrium with Sr^{2+} in the feed simulant, a 'bleed' of Sr^{2+} is observed with concentrations up to 20% greater than that of the feed measured in the column eluant. The concentration of Sr^{2+} in the

eluant remains above that of the feed concentration for ca. 1000 BV before C_o/C returns to unity.

One explanation for the 'bleed' of Sr^{2+} from the fixed-bed is that under the dynamic conditions of the fixed-bed column experiment, Sr^{2+}-loaded composite adsorbent is constantly in contact with fresh acidic simulant, possibly resulting in desorption of Sr^{2+} from the stationary phase by hydronium ions viz. H_3O^+ leaching. Another explanation might involve competitive desorption of Sr^{2+} by Cs^+ in the fresh feed simulant, by virtue of the greater selectivity of the MoHTB adsorbent for Cs^+ over Sr^{2+} (7, 8). In an attempt to discern between these two possible scenarios, the Sr^{2+} breakthrough profiles for the MoHTB-PAN-80-D (<0.3 mm) composite adsorbent were determined using acidic feed solutions containing Sr^{2+} ($0.375\ mmol \cdot L^{-1}$) and varying levels of Cs^+ (0, 0.94, or $2.25\ mmol \cdot L^{-1}$) (Fig. 6). The concentrations of Sr^{2+} and Cs^+ in these feed solutions were employed to ensure rapid breakthrough (relative to the original radwaste simulant) of Sr^{2+} from the fixed-bed setup, and facilitate rapid assessment of the column performance data, k_1 and q_0, for Sr^{2+} adsorption by the composite adsorber fixed-bed. The Sr^{2+} breakthrough plots in Fig. 6 demonstrate that in the absence of Cs^+ a typical 'S' shaped breakthrough profile is observed, with no "bleed" of Sr^{2+} into the column effluent. This indicates that once the composite fixed-bed is at equilibrium with the feed solution, the Sr^{2+}-loaded composite is not affected by the continued passage of "fresh" acidic solution through the column. For the alternative feed solutions containing increased concentrations of Cs^+, a concomitant increase in the degree of Sr^{2+} "bleed" is observed from the composite fixed-bed, therefore implying that the proposed desorption mechanism

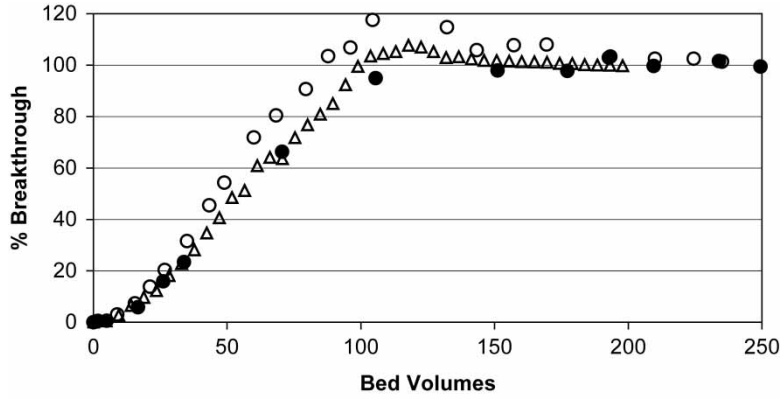

Figure 6. Breakthrough profiles of Sr^{2+} for MoHTB-PAN-80-D composite fixed-bed columns using acidic feed solutions containing a fixed concentration of Sr^{2+} ($0.375\ mmol \cdot L^{-1}$ in 1.0 M HNO_3) and various concentrations of Cs^+ ($0\ mmol \cdot L^{-1}$ ●; $0.094\ mmol \cdot L^{-1}$ △; $0.225\ mmol \cdot L^{-1}$ ○); BV = ca. 1.8 ml; F = $30\ BV \cdot h^{-1}$.

involving Cs^+ is at play after the composite fixed-bed is at equilibrium with respect to strontium. These results also make it quite apparent that the capacity for Sr^{2+} and degree of "bleed" of Sr^{2+} from the composite fixed-bed are dependent on the concentration of Cs^+ present in the acidic feed solution.

The complexities associated with modeling the adsorption of a fixed-bed column are well documented (17–19) but the simplified model originally proposed by Thomas (20) has been successfully employed by several investigators. In brief, the model can be described by Eq. (4) where axial dispersion is neglected, the effects due to diffusion are combined into one constant, k_1, and where C = cation effluent concentration ($mg \cdot L^{-1}$); C_o = cation feed concentration ($mg \cdot L^{-1}$); k_1 = column exhaustion rate constant ($L \cdot h^{-1} \cdot mg$); F = flow rate ($L \cdot h^{-1}$); q_o = equilibrium adsorbent phase cation concentration ($mg \cdot g^{-1}$); M = mass of composite adsorbent (g); and V = eluant volume (L). The overall rate constant, k_1, and cation capacity, q_o, can be calculated from either a regression fit of the C_o/C vs. V (L) plot, or from the linearized form of Eq. (4) [Eq. (5)].

$$\frac{C_o}{C} = 1 + e^{k_1/F(q_oM - C_oV)} \tag{4}$$

$$\ln\left(\frac{C_o}{C} - 1\right) = \left(\frac{k_1 C_o V}{F}\right) + \left(\frac{k_1 q_o M}{F}\right) \tag{5}$$

Employing the later analysis, the breakthrough profiles for Cs^+ and Sr^{2+} with the MoHTB-PAN-80-C and -D composites using radwaste simulant (Table 3); and for Sr^{2+} with various levels of Cs^+ with the MoHTB-PAN-80-D composite (Table 4), were analyzed to derive the overall rate constants (k_1) and column capacity values (q_o). In the case of the radwaste simulant feedstock, the Cs^+ and Sr^{2+} capacity values calculated by this treatment are comparable for both composites and are as expected given that the two materials only differ with respect to their size fraction, and not their chemical composition. Furthermore, the calculated q_o for Cs^+ and Sr^{2+} are in reasonable agreement with the maximum cation uptake

Table 3. Overall rate constant (k_1) and dynamic cation exchange capacity (q_o) for MoHTB-PAN-80-C and -D composite fixed-bed columns using acidic radwaste simulant

	k_1 ($L \cdot h^{-1} \cdot mg^{-1}$)		q_o ($mg \cdot g^{-1}$)	
	Cs^+	Sr^{2+}	Cs^+	Sr^{2+}
MoHTB-PAN-80-C	0.119	0.395	8.89	1.66
MoHTB-PAN-80-D	0.088	0.409	8.91	1.60

Table 4. Overall rate constant coefficient (k_1) and dynamic cation exchange capacity (q_o) of MoHTB/PAN-80-D composite fixed-bed column sorption of Sr^{2+} using feed solutions containing variable concentrations of Cs^+

	Sr^{2+} k_1 $(L \cdot h^{-1} \cdot mg^{-1})$	Sr^{2+} q_o $(mg \cdot g^{-1})$
$0\,mmol \cdot L^{-1}$ Cs^+	0.0559	6.664
$0.375\,mmol \cdot L^{-1}$ Cs^+	0.0445	6.947
$2.25\,mmol \cdot L^{-1}$ Cs^+	0.0764	4.783

$(mg \cdot g^{-1})$ predicted from the Langmiur fits of the adsorption isotherms for MoHTB-PAN-80-D and the cesium and strontium-containing radwaste simulant (Fig. 7). For the Sr^{2+} breakthrough profiles observed with feedstocks containing varying levels of Cs^+ the susceptibility of a portion of adsorbed Sr^{2+} to desorption by Cs^+ in the feed solution is reflected in the values of k_1 and q_o (Table 4) with the overall rate coefficient increasing by ca. 30% and the capacity for Sr^{2+} decreasing by 38% at the maximum concentration of Cs^+ studied.

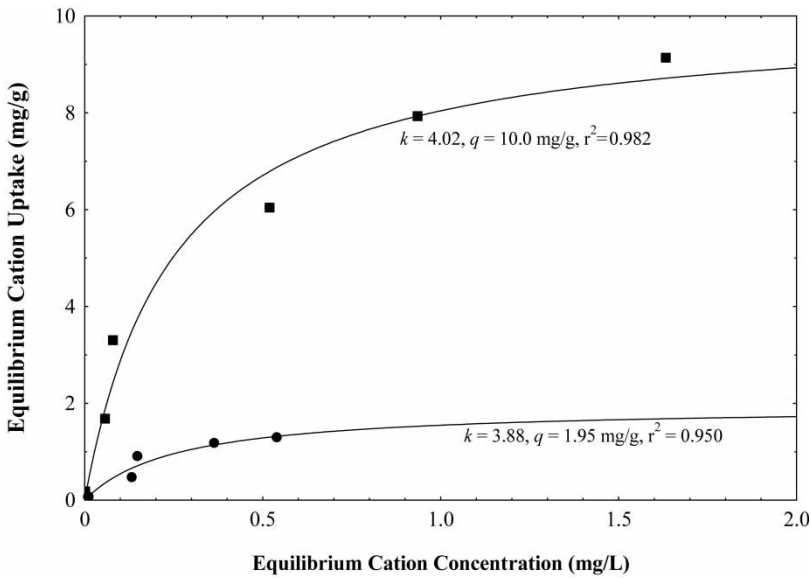

Figure 7. Equilibrium cation uptake (mg/g) of MoHTB-PAN-D composite for Cs^+ (■) and Sr^{2+} (●) using acidic radwaste simulant (ca. $0.075\,mmol \cdot L^{-1}$ Cs^+ and Sr^{2+} in 1.0 M HNO_3).

In the absence of more rigorous numerical treatment of the breakthrough data, the ability to describe the Cs^+ and Sr^{2+} breakthrough performance of the composite fixed-beds in part validates the use of the Thomas model to describe the individual adsorption of Cs^+ and Sr^{2+} by the fixed-bed up to ca. 90–95% breakthrough. Given that the Thomas model was originally formulated to describe the adsorption of a single species from solution, the apparent applicability of the model might be seen to infer that the ion-exchange of Cs^+ and Sr^{2+} by the composite occurs by two independent mechanisms, or in other words, at two distinct sites within the MoHTB structure. However, the results presented in Fig. 6 demonstrate that this is not strictly the case as some Sr^{2+} is susceptible to ion-exchange/desorption by Cs^+, and that k_1 and q_o column performance parameters are specific for given feedstock solutions. Furthermore, comparison of the calculated Cs^+ and Sr^{2+} q_o values from the modeling should be made against the cation exchange capacities derived from the adsorption isotherm for the corresponding Cs^+ and Sr^{2+}-containing feedstock solution, and not the individual binary (Cs^+/H^+ or Sr^{2+}/H^+) adsorption isotherms.

The calculated k_1 and q_o values for the two composites were subsequently employed at varying elution volumes (expressed in terms of BV) to generate theoretical Cs^+ and Sr^{2+} breakthrough profiles for the MoHTB-PAN-80-C and -D composites with acidic radwaste simulant using Eq. (4) (Fig. 8). For the Cs^+ and Sr^{2+} breakthrough profiles of the MoHTB-PAN-80-C composite and Sr^{2+} breakthrough profile of the MoHTB-PAN-80-D composite there is excellent agreement (neglecting the 'bleed' of Sr^{2+})

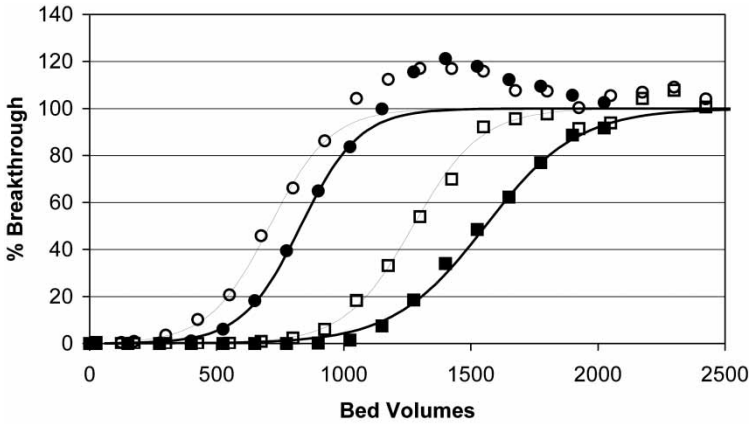

Figure 8. Experimental and theoretical breakthrough profiles of Cs^+ and Sr^{2+} for MoHTB-PAN-80-C and -D composite fixed-bed column with acidic radwaste simulant (ca. 0.075 mmol $\cdot$ L^{-1} Cs^+ and Sr^{2+} in 1.0 M HNO_3); BV = ca. 0.8 mL; Flow rate = 30 BV $\cdot$ h^{-1}; Legend: MoHTB-PAN-80-C Cs^+ and Sr^{2+} (□ and ○, respectively); MoHTB-PAN-80-D Cs^+ and Sr^{2+} (■ and ●, respectively).

between the theoretical and experimental profiles. The theoretical and experimental Cs^+ breakthrough profiles of the MoHTB-PAN-80-D composite are also in good agreement; however the model marginally underestimates the composite's sorption of Cs^+ in the early stages (1–10%) of Cs^+ breakthrough.

CONCLUSIONS

Granulation of the inorganic phase, $Na_{0.2}Mo_{0.03}W_{0.97}O_3 \cdot ZH_2O$ (MoHTB), with PAN affords a composite adsorbent which can be successfully deployed in fixed-bed (1 mL) column separations of Cs^+ and Sr^{2+} from acidic radwaste simulants. It is clear that as the bead size of this composite is decreased the polyacrylonitrile matrix has increasingly less impact upon the kinetics of Cs^+ and Sr^{2+} uptake by the MoHTB phase which has previously been shown to be quite rapid. In addition, further scope exists to potentially improve the Cs^+ and Sr^{2+} adsorption kinetics of the composite materials by avoiding drying during their processing as has been found in the case of the AMP-PAN-85 composite adsorbent.

The breakthrough profiles of Cs^+ and Sr^{2+} from acidic radwaste simulant using the two smallest bead size fractions of MoHTB-PAN-80 have been successfully described using the simplified model proposed by Thomas. Although the modeling has been successfully conducted for each cation independently, this approach masks the subtle interplay between the two adsorption processes. The adsorption of Cs^+ and Sr^{2+} by the MoHTB-PAN-80 composites in a fixed-bed column setup appears to occur by two independent processes where the molar ratio of Cs^+:Sr^{2+} falls below 0.25:1. Above this point, the Sr^{2+} dynamic cation exchange capacity (q_0) and overall rate coefficient (k_1) for the composite column are highly dependent on the concentration of Cs^+ present. Thus demonstrating that any column performance data derived for a given feedstock solution is specific to that feedstock solution.

ABBREVIATIONS AND SYMBOLS

AMP	ammonium molybdophosphate
BV	bed volume
C_i	initial cation concentration in static batch experiments ($mg \cdot L^{-1}$)
C_f	final cation concentration in static batch experiments ($mg \cdot L^{-1}$)
C	cation concentration in column effluent ($mg \cdot L^{-1}$)
C_o	cation concentration in column feed ($mg \cdot L^{-1}$)
CST	crystalline silico-titanate
F	flow rate ($L \cdot h^{-1}$)
h	rate of cation adsorption as $t \rightarrow 0$ min ($mg.g^{-1} \cdot min$)

k	Langmuir adsorption coefficient
k_1	column exhaustion rate constant for a given cation ($L \cdot h^{-1} \cdot mg$)
k_{ad}	overall rate of cation adsorption ($g \cdot mg^{-1} \cdot min$)
M	mass of composite adsorbent in the fixed-bed column (g)
MoHTB	molybdenum-doped hexagonal tungsten bronze
PAN	polyacrylonitrile
q	equilibrium adsorbent phase cation concentration ($mg \cdot g^{-1}$)
q_o	dynamic cation exchange capacity ($mg \cdot g^{-1}$)
t	time for adsorption (min)
V	volume of feed passed through a fixed-bed column (L)

REFERENCES

1. Clearfield, A. (2000) Inorganic ion exchangers, past, present, and future. *Solvent Extraction and Ion Exchange*, 18 (4): 655.
2. Todd, T.A., Brewer, K.N., Law, J.D., Wood, D.J., Garn, T.G., Tillotson, R.D., Tullock, P.A., and Wade, E.L. (1997) Development and Application of Separation Technologies for the Treatment of Radioactive Wastes. In Waste Management conference, Tuscon; 2368.
3. Poojary, D.M., Cahill, R.A., and Clearfield, A. (1994) Synthesis, crystal structures, and ion-exchange properties of a novel porous titanosilicate. *Chem. Mater.*, 6 (12): 2364.
4. Luca, V., Hanna, J.V., Smith, M.E., James, M., Mitchell, D.R.G., and Bartlett, J.R. (2002) Nb-substitution and Cs^+ ion-exchange in the titanosilicate sitinakite. *Microporous and Mesoporous Materials*, 55 (1): 1.
5. Fondeur, F.F., Walker, D.D., Wilmarth, W.R., and Fink, S.D. (2001) The effect of pressure, humidity, caustic pretreatment, and organic constituents on the cesium ion exchange performance of IONSIV IE-911. *Sep. Sci. and Technol.*, 36 (16): 3599–3615.
6. Wilmarth, W.R., Hang, T., Walker, D.D., Mills, J.T., Dukes, V.H., and Fink, S.D. (2000) Cesium removal from SRS high-level waste using crystalline silicotitanate-ion exchange, 2000; Abstract of papers, IEC 254, 219th ACS National Meeting, San Francisco, CA, March 26–30, American Chemical Society: Washington, DC, 2000.
7. Luca, V., Griffith, C.S., Chronis, H., Widjaja, J., and Scales, N. (2003) Ion-exchange properties of microporous tungstates. *MRS Proceedings—Scientific Basis for Nuclear Waste Management*, XXVII: 309–314.
8. Griffith, C.S. and Luca, V. (2004) Ion-exchange properties of microporous tungstates. *Chem. Mater.*, 16 (24): 4992–4999.
9. Sebesta, F. Preparation of granular forms of powdered materials for their application in column packed beds. NATO Science Series, Series E: Applied Sciences, 1999, 362, (Natural Microporous Materials in Environmental Technology), 473–486.
10. Reis, K.P., Ramanan, A., and Whittingham, M.S. (1990) Hydrothermal synthesis of sodium tungstates. *Chem. Mater.*, 2 (3): 219–221.
11. Reis, K.P., Prince, E., and Whittingham, M.S. (1992) Rietveld analysis of sodium tungstate hydrate $Na_xWO_{3+x/2} \cdot yH_2O$, which has the hexagonal tungsten bronze structure. *Chem. Mater.*, 4 (2): 307–312.

12. Luca, V. Inorganic ion exchangers for removing contaminant metal ions from liquid streams. WO Patent 0296559, May 31, 2002.
13. Sebesta, F. Sorbent composed of active component and binding organic matrix and method of its production. CS Patent 273369, January 21, 1992.
14. Kim, H.T., Lee, C.H., Shul, Y.G., Moon, J.K., and Lee, E.H. (2003) Evaluation of PAN-TiO_2 composite adsorbent for the removal of Pb(II) ions in aqueous solutions. *Sep. Sci. and Technol.*, 38 (3): 695–713.
15. Sebesta, F., John, J., Motl, A., and Stamberg, K. (1995) Evaluation of PAN as a binding polymer for absorbers used to treat liquid radwaste: Phase I. Report SAND95-2729. Sandia National Laboratories: Albuquerque, New Mexio.
16. Ho, Y.S., Wase, D.A.J., and Forster, C.F. (1996) Kinetic studies of competitive heavy metal adsorption by sphagnum moss peat. *Environ. Technol.*, 17: 71–77.
17. Ruthven, D.M. (1984) *Principles of Adsorption and Adsorption Processes*; Wiley: New York.
18. Helfferich, F. (1962) *Ion Exchange*; McGraw-Hill Book Company: New York.
19. Tranter, T.J., Herbst, R.S., and Todd, T.A. (2002) Determination of a solid phase mass transfer coefficient for modeling an adsorption bed system using ammonium molybdophosphate-polyacrylonitrile (AMP-PAN) as a sorbent for the removal of ^{137}Cs from acidic nuclear waste solutions. *Adsorption*, 8 (4): 291–299.
20. Thomas, H.C. (1948) A problem in kinetics. *Anals. of the New York Academy of Science*, 49: 161.